PURPOSE-LED
PUBLISHING™

PAPER

Electrochemical corrosion performance of friction stir processed cold spray metal matrix composite coatings on AZ31B magnesium alloy under sodium chloride environment

To cite this article: Ashokkumar Mohankumar *et al* 2022 *Surf. Topogr.: Metrol. Prop.* **10** 035010

View the article online for updates and enhancements.

Surface Topography: Metrology and Properties

PAPER

Electrochemical corrosion performance of friction stir processed cold spray metal matrix composite coatings on AZ31B magnesium alloy under sodium chloride environment

Ashokkumar Mohankumar[1,*] ⓘ, Thirumalaikumarasamy Duraisamy[1], Deepak Sampathkumar[2] ⓘ and Tushar Sonar[3]

1   Department of Manufacturing Engineering, Annamalai University, Annamalai Nagar, Chidambaram-608002, Tamil Nadu, India
2   Department of Mechanical and Automation Engineering, Agni College of Technology, Thalambur, Chennai-600130, Tamil Nadu, India
3   Department of Mechanical Engineering, G. S. Mandal's Maharashtra Institute of Technology, Aurangabad 431010, Maharashtra, India
*   Author to whom any correspondence should be addressed.

E-mail: ashokleadsaero12@gmail.com

Abstract

The main objective of this investigation is to study the effect of friction stir processing (FSP) on the surface integrity and corrosion resistance of low-pressure cold sprayed (LPCS) aluminium alloy/ aluminium oxide metal matrix composite (Al-Al$_2$O$_3$ MMC) coating deposited on AZ31B magnesium alloy for aerospace and automobile applications. The Al-Al$_2$O$_3$ MMC coating was developed on AZ31B magnesium alloy using a LPCS system. FSP was performed on the MMC coating using a stirring tool made of H13 tool steel. The structural integrity of the coating was analyzed using scanning electron microscopy (SEM). The phase analysis of coating was studied using x-ray diffraction (XRD). The potentiodynamic polarization and electrochemical impedance spectroscopy (EIS) tests were performed to study the corrosion resistance of cold sprayed and FSPed samples. Results showed that FSP improved the structural integrity of MMC coating. Both the EIS and potentiodynamic polarisation test results reveal that FSP treated samples provide superior corrosion resistance than cold sprayed samples. This is due to the increase in interfacial bonding between matrix and reinforcement phase. The degree of separation and dispersal of alumina in the Al alloy matrix is increased through the shear force generated by the FSP tool on the coating surface.

1. Introduction

AZ31B magnesium alloy is a light material with high specific strength and thermal conductivity. It has been used in many automobiles, aerospace and various industries, but its application has been very limited owing to its poor corrosion resistance [1, 2]. To overcome this issue, cold spray (CS) has gained popularity due to its solid form of coating development for various industrial applications [3]. In this method, the substrate was exposed to supersonic velocity coating materials propelled through an expanded process gas at lower temperatures than that of the coating powder melting temperature [3]. These parameters characterise CS as a lower temperature, higher velocity method with the notable merit of no oxidation or phase transition, allowing the coating

material to keep its original characteristics [4–6]. In comparison with other popular coating methods (high velocity oxy fuel and atmospheric plasma spray), bonding in CS occurs in a solid state with a plastically deformed state instead of melting at extremely elevated temperatures [7–10]. Because of these benefits, it can be used to produce various reinforcements of the ceramic element metal matrix composites (MMCs) such as Al 5056-SiCp [11], aluminium-alumina [12], and Cu-CNT-SiC [13]. Spencer *et al* [12] investigated Al/alumina coatings on the AZ31B Mg alloy. The addition of reinforcement elements in MMCs will improve the plastical deformation of the metallic phase. It results in the reduction of coating porosity, enhancing hardness and electrochemical behaviour compared with CS metallic materials and alloys [11–14]. Some of the ceramic elements were

destroyed due to their high-velocity impact, but the interface bonding between the matrix and reinforcement phase was lower. As a result, the MMC's corrosion resistance has a native effect on electrochemical performance.Yu *et al* [11] investigated Al5056-SiCp coatings on aluminium substrates by changing the volume percentage (15,30,45, and 60) of the reinforcement. The result revealed that the mechanical and tribological behaviour of the coatings was greatly improved compared to the aluminium substrate. This is due to the presence of ceramic particles in the deposit. The same phenomena were obtained by Xiang *et al* [15], who examined the A380/ alumina MMC composite coatings on AZ31 Mg alloy. Chen Xie *et al* [16] examined the electrochemical behaviour of the zinc deposit on the AZ31B magnesium alloy through the cold spray process. As a result, the corrosion resistance of the zinc coated sample was greatly improved compared with the base substrate (AZ31B Mg alloy). But the corrosion tunnel was developed in the cross-sectional region of the coating. Richard Gawel *et al* [17] examined the oxidation performance of the silicon coatings on the four different steel valves. They revealed that the corrosion resistance of the steel was highly improved for the coated samples compared to the uncoated samples. This is owing to the development of the protective MnCr2O4 on the coated samples. Heat treatment is one of the popular methods to enhance the bond strength between the metal particles of the deposit [18]. But this condition is not effective for MMC coatings because the reinforcement element remains in the larger size even after the heat treatment process. This makes it extremely challenging to enhance poor interfacial bonding between reinforced and metal particles [7, 15]. As a result, cold sprayed coatings require a post-treatment. The environmentally friendly solid-state technique, friction stir processing (FSP), has been utilised to change the microstructural characteristics of any metallic surface [16, 17]. A rotational stirring tool is inserted into the surface of the work piece and it moves around the specimen surface through stirring action which develops the frictional heat on the surface of the work piece and extreme plastic deformation at higher strain.

The FSP has been utilised for the refination of the reinforced particles and to eliminate the weaker interaction among the particles in cold sprayed MMCs [19–23]. The study reveals that the particles were redistributed and refination occurred on the work piece. These properties lead to an improvement in the corrosion resistance of the MMC coatings [23]. Khodabakhshi *et al* [20] examined the cold sprayed AA7075 deposit on the AZ31B Mg alloy followed by FSP. The hardness of the coating was greatly enhanced after FSP, compared to the base substrate. This is due to the plastical deformation and refining of the particles in the coating surface during FSP. Hodder *et al* [21] developed the cold sprayed aluminium/alumina MMC deposit on the aluminium alloy (grade: 6061)

substrate followed by FSP. After FSP, the deposit microhardness (137 HV) improved compared to the cold sprayed and the base substarte samples. This enhancement is due to the re-distributed alumina particles into the matrix phase with refining of the particle size. C.J. Huang *et al* acknowledged similar behaviour in the fabrication of SiCp/Al5056 MMC coatings using friction stir processing [22]. KangYang *et al* [23] investigated the corrosion behaviour of the cold sprayed Al alloy (AA2024)/Al$_2$O$_3$ MMC coatings on the aluminium alloy substrate through friction stir processing by changing the pass numbers (1st, 2nd, and 4th) of the FSP. They revealed that the lower pass number of FSP samples shows better corrosion resistance compared to the higher pass number (4th pass) and the cold sprayed samples.

Many researchers have investigated the mechanical and corrosion performance of cold sprayed coatings and their microstructural analysis. But the electrochemical corrosion behaviour of post treatments on cold sprayed MMC coating on magnesium alloy and its electrochemical properties have not been studied up to now. The present study focuses on improving the corrosion resistance of AZ31B magnesium alloy using low pressure cold sprayed MMC coatings with friction stir processing. This improved AZ31B Mg alloy with aluminium alloy/aluminium oxide MMC coating followed by FSP can meet realtime applications in industries such as aviation (helicopter rotor fittings and aircraft engine mounts) and automobiles (engine blocks and housing for transmissions).

2. Materials and methods

Figure 1(a) illustrates the SEM images of the aluminium alloy powder spherical in shape, and figure 1(b) demonstrates the fused crushed Al oxide powder. The particle size of the aluminium alloy and aluminium oxide powders was 60 ± 7 μm and 50 ± 8 μm respectively, and the composition of the powder are shown in table 1. The coating materials were blended using a tubular mixer with a volumetric ratio of 4:1. AZ31B Mg alloy was used as the coupon, with a thickness of 5 mm. Before coating, the substrate was cleaned using ethanol and sand blasting (shot plaster, SB P7 150, Bangalore, India) was done using alumina with a grit size of 250 ± 400 μm and a pressure of 40 bar to improve the roughness of the substrate [3]. The surface roughness of the substrate was about Ra = 4 μm. It was measured using the surface roughness tester (Mitutoyo, SJ210, Tokyo, Japan) in order to increase the adhesion between the coating and substrate. The MMC coating was fabricated using a low-pressure cold spray system (Dymet423, Russia) with optimized process parameters as illustrated in table 2.

After the cold spray process, the friction stir processing was done on the surface of the coating using a
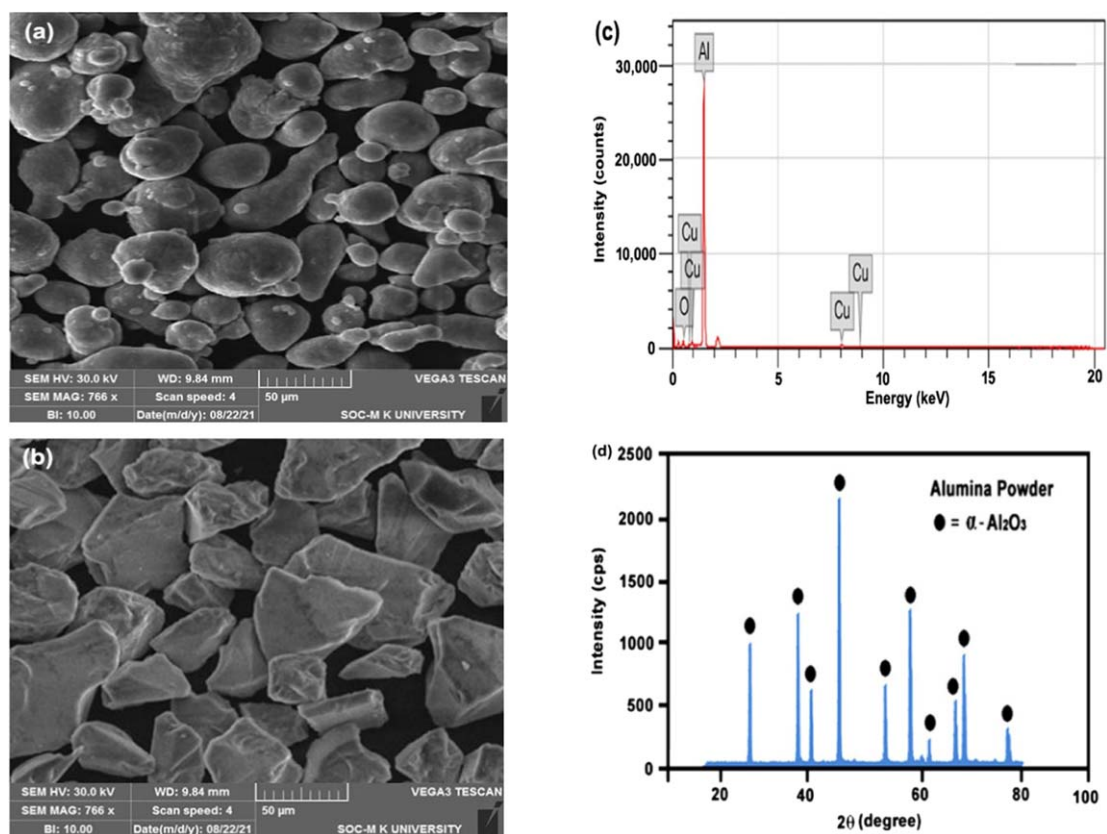
Figure 1. (a), (b) SEM morphology of spray powders (a) aluminium alloy powder (b) aluminium oxide powder (c) EDS report of aluminium alloy powder (d) XRD report of aluminium oxide powder.

friction stir welding setup (RS Machine Tools, Bangalore, India) as shown in the figure 2. Friction stir processing was carried out using an H13 steel stirring tool. The dimension of the tool and the optimised parameters of the FSP are illustrated in tables 3 and 4. After FSP, the electrochemical experiments were performed using potentio-dynamic polarization and electrochemical impedance spectroscopy (EIS). The three-electrode electrochemical setup was utilized. The reference electrode is a saturated calomel electrode, the counter is a platinum electrode, and the MMC coating is the working electrode. Before the experiment, the samples were cleaned and masking was applied to the uncoated region in the sample through epoxy resin. The experiment was conducted for one hour at the open circuit potential. To stabilise the samples, they were immersed in a 3.5 weight percent sodium chloride solution for an hour. The EIS graph was attained by applying 9.5 mV alternative current amplitude ranges from 9 Hz to 100 kHz. The polarisation scan was initiated at 500 mV of the OCP and raised at a rate of 2 mV s^{-1} to +1400 mV of the OCP. To verify repetition, every specimen was analysed five times in the same state. The results were examined through Z-sim Demo software.

The surface morphology of the coating materials and coatings was studied using scanning electron microscopy (JEOL, 6410-LV, Tokyo, Japan). The

Table 1. Chemical composition (wt%) of AA2024 Al alloy coating material.

Cu	Mg	Mn	Al
4.3	1.3	0.3	Balance

Table 2. LPCS coating parameters.

Sr No	Parameters	Values
1.	Processing gas	Air
2.	Pressure	10 bar
3.	Temperature	540 °C
4.	Powder feed rate	23 gram min^{-1}
5.	Spray distance	20 mm

phase behaviour was obtained through XRD (ULTIMA-II, Rigak, Japan) with a step resolution of 0.00300. The precipitation of aluminium was obtained by differential scanning calorimetry (DSC) (TA Instruments,DSC240, India). It was conducted under argon with a heat range of 5 to 420 °C min^{-1}. The porosity of the as sprayed and FSPed samples was measured using an optical microscope (Radical, RAD-800B India) integrated with image analysis software (Metal Vison 9). Microhardness tests were carried out using a Vickers microhardness tester (Shimadzu,
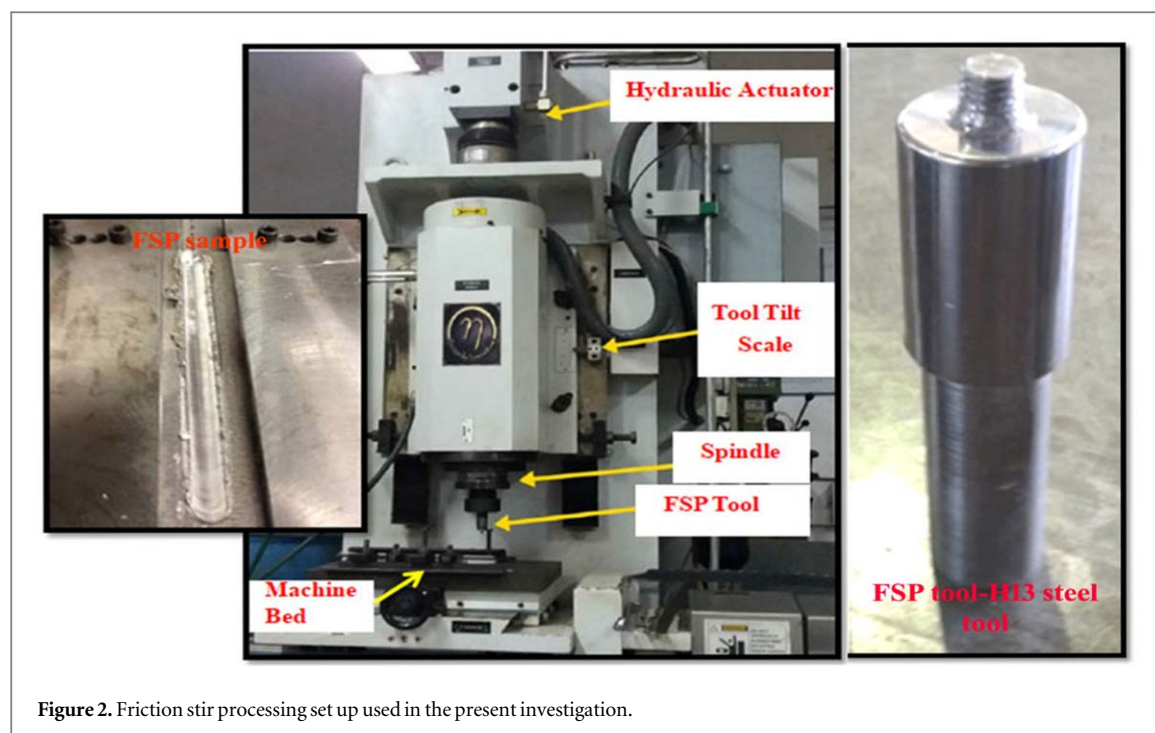
Figure 2. Friction stir processing set up used in the present investigation.

Table 3. Dimension of the FSP tool made of H13 tool steel.

Root diameter	Root length	Concave shoulder diameter
3 mm	2 mm	15 mm

Table 4. Optimized parameters of the FSP employed in this investigation.

Rotational Speed (rpm)	Transverse speed (mm min)$^{-1}$	Concave shoulder tilt angle (degree)
850	40	2

HMV-2T, Japan). The adhesion strength was measured using the tensile testing machine (BEV Blue Sun, TTM 203, India).
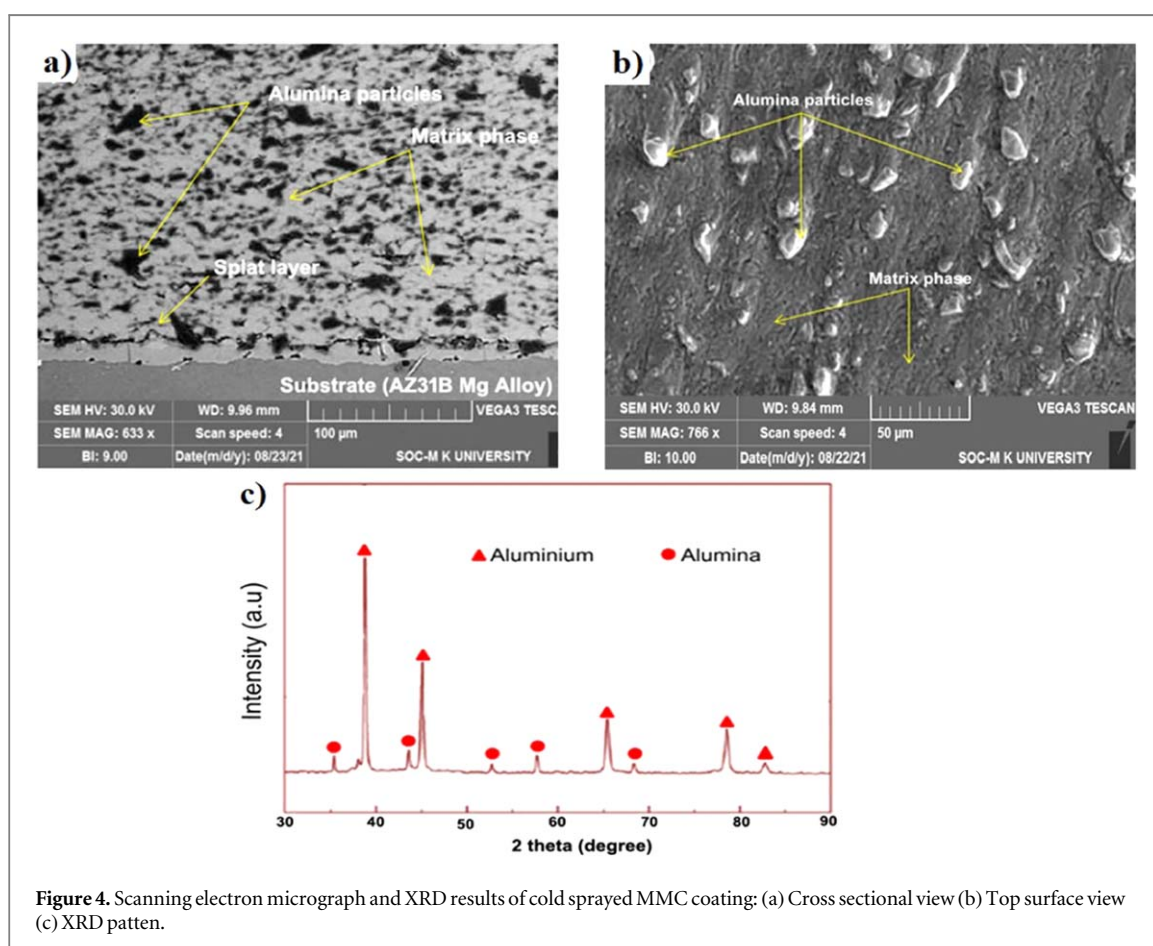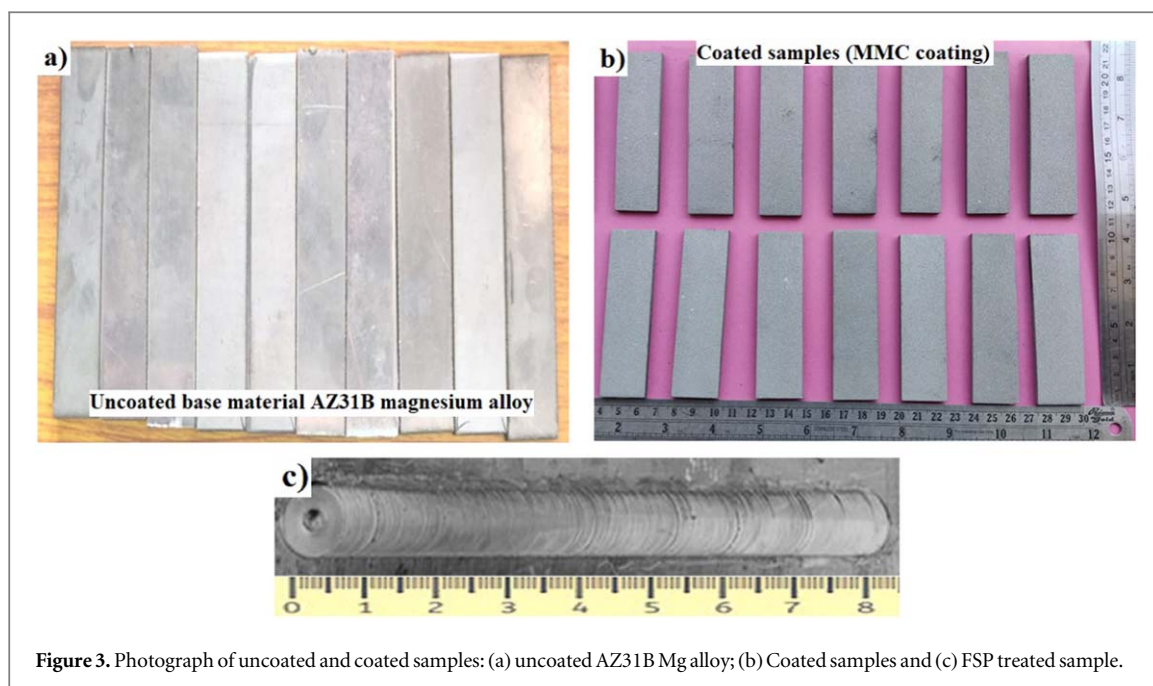
3. Result and discussion

3.1. Coating characterization

Figure 3 illustrates the photo graph view of the uncoated substrate (AZ31B Mg alloy), cold sprayed MMC coatings and after FSP treated sample. The microstructural image of the low-pressure cold-sprayed MMC coating is shown in figures 4(a) and (b). The vast majority of the dark region was alumina elements. A few alumina elements were smashed into small sizes due to the high velocity impact [11]. The adhesive behaviour between the deposit and the base material was excellent. Due to the surface roughness created by sand blasting and also the high velocity impact of the coating materials through the cold spray nozzle [12], the cohesive behaviour of the deposit was

not better because the interface bonding between the alumina elements and the matrix phase was a little weaker [15]. There were small pores and voids between the interface of the matrix and the ceramic phase.

For the porosity evaluations, metallographically cross-sectioned coated and FSP samples were prepared. A slower run metallurgical cutting tool (Make: Ducom, WER01, India) comes with an epoxy diamond cutter tool and was used to precisely cut both the sprayed and FSP samples to their required sizes. The samples were placed in a vacuum in the lower viscous epoxy adhesive. The placed samples were grounded using 500, 800, 1200, and 1400 grit silicon sheets and polishing was done using diamond slurry of 12–10, 10–4, 4–2, 2–3, and 3–0.5 μm for 4, 6, 8, 12, and 13 min According to ASTM B 276, the porosity of the as sprayed and FSP cross-sectional samples was measured using an optical microscope integrated with image analysis software. The cross-sectional samples of the as sprayed and FSP were below 800x and were taken for porosity examination to evaluate the pores and cracks in the as sprayed and FSP samples. A 700 μm squared area was picked to examine the coating characteristics. The experimentation was repeated six times in order to get the average percent of porosity. A few pores were identified between the interface of the matrix and the reinforcement phase of the coated sample. The porosity level was approximately 4%. When compared to the cold sprayed state, the porosity of the FSP sample was lowered by 0.5 percent, as shown in figure 5. This is because the degree of separation and dispersal of alumina in the Al alloy matrix was increased and refining of the alumina elements occurred through the shear force generated by the FSP tool on the coating surface.

Figure 3. Photograph of uncoated and coated samples: (a) uncoated AZ31B Mg alloy; (b) Coated samples and (c) FSP treated sample.

Figure 4. Scanning electron micrograph and XRD results of cold sprayed MMC coating: (a) Cross sectional view (b) Top surface view (c) XRD patten.

Microhardness tests were carried out using a Vickers microhardness tester. The indention mark was made on the cross sections of the as sprayed and FSP samples under a 350 gram load for 20 s. The measurement sequence for both coated and FSP specimens consisted of 10 random indentations. The coating hardness of the as sprayed sample was about 135 HV and the hardness of the FSP sample was highly increased to 155 HV, as shown in figure 6 [16–21]. By dispersing and reducing the mean free path of alumina elements, FSP improves the hardness of MMC coatings remarkably [19]. The ASTMC-633–01 standard
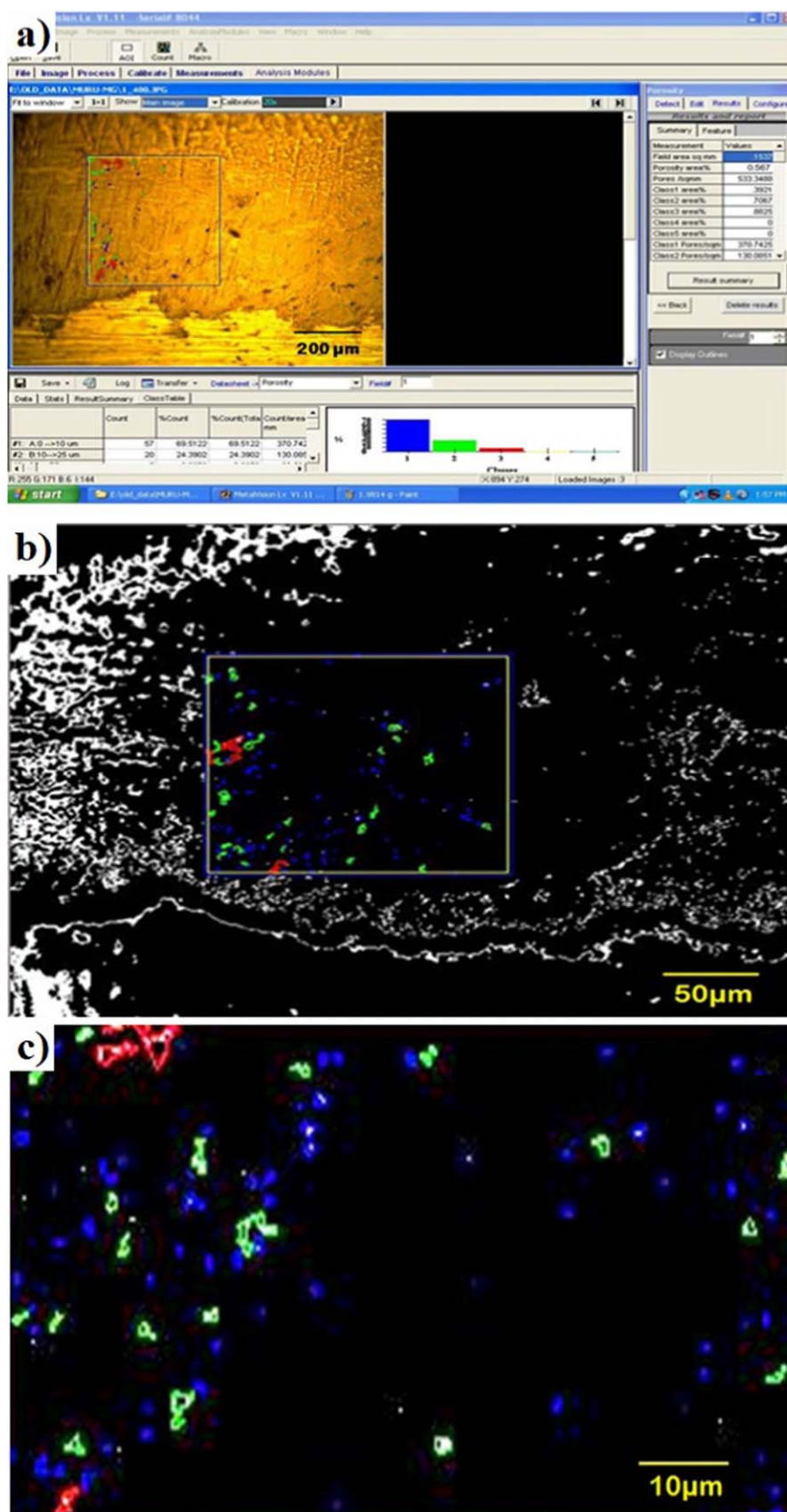
Figure 5. Steps involved in image analysis FSP of sample: (a) Binary image of the selected image; (b) Selection of region to be examined (c) Colour coded image after porosity evaluation.
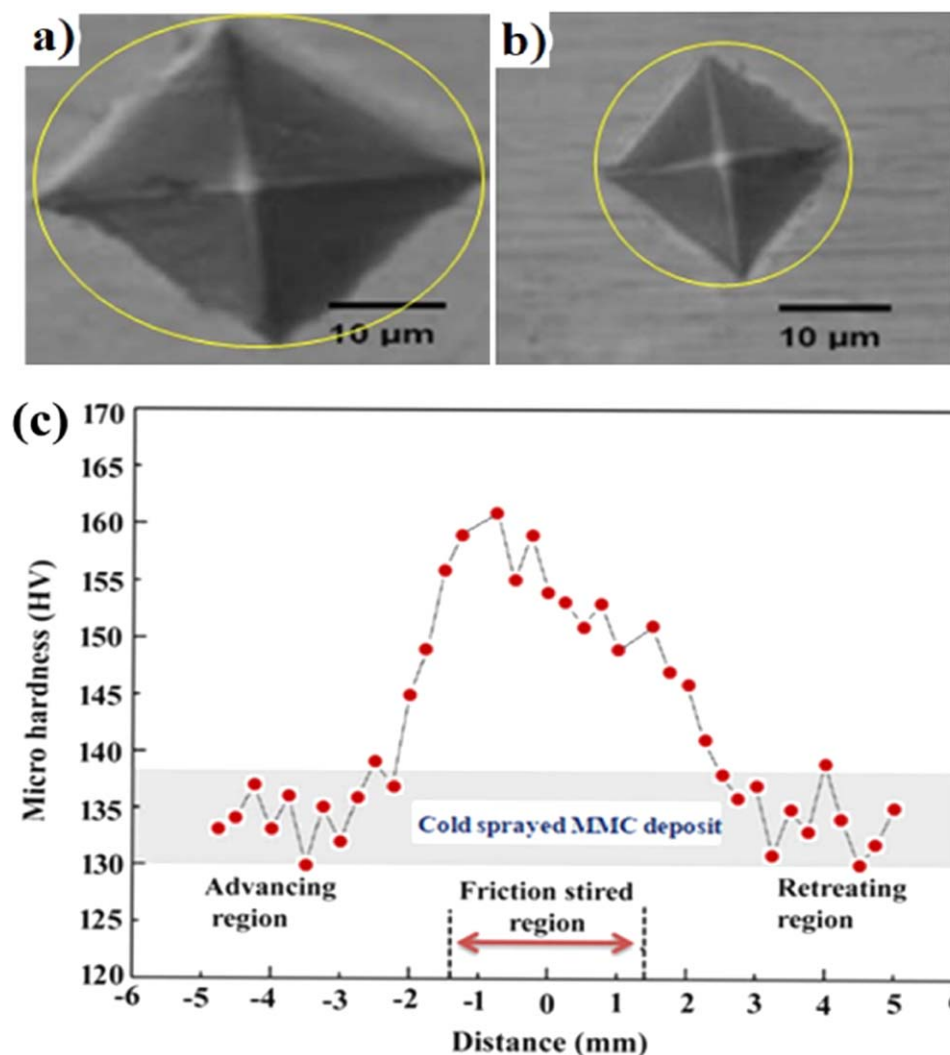
Figure 6. Indention morphology on samples: (a) as coated sample (b) FSP treated sample and (c) Microhardness survey of MMC deposit.

[24] was used to assess the adhesion strength of the deposit. The coated sample was attached to stainless steel 316 using E9-adhesive. After solidification, the measurement was conducted using a tensile testing machine. The crosshead velocity of the apparatus was 2 mm min^{-1}. The adhesion strength of the sample was about 50 MPa.

The alumina element refining was superior as shown in the figures 7(a) and (b) [21, 23]. The voids in the deposit were reduced and the interface voids between the alumina and the Al alloy phase disappeared. It results in the reduction of porosity with better enhancement of the mechanical properties [22]. The degree of separation and dispersal of alumina in the Al alloy matrix was increased with the greater refining of alumina particles, but some ceramic elements were retained in larger sizes. The refination is owing to the shear forces produced by the FSP tool when it is stirred on the MMC coatings. The FSP not only refines the coating surface but also plastically reforms the coating surface due to the thermo-mechanical process of the FSP. Even though a

homogeneous MMC coating was developed after FSP with the break of the alumina elements [15]. The XRD plots in figures 4(c) and 7(c) show that the peaks associated with alumina particles were reduced after FSP when compared to cold sprayed specimens, and the JCPDS card no. for aluminium: 85–1327 and for alumina: 10–0173. This refining occurred through the shear force generated by the FSP tool on the coating surface. interface bonding between the matrix and the reinforcement phase was improved [21–25].

The aluminium oxide dispersion is irregular, with a higher range of splitting in the top and bottom areas of the friction stirred specimen. This is attributed to material movement and stirring operations produced via the FSP tool. The interaction bonding among the metal elements in the cold sprayed deposit acts as the preferable area for localised corrosion [23]. Even though the presence of aluminium oxide in cold sprayed MMC coatings was anticipated to lower the area that can be assaulted by an electrolyte, the assault on the aluminium oxide elements was stronger because of the weak interface bond between
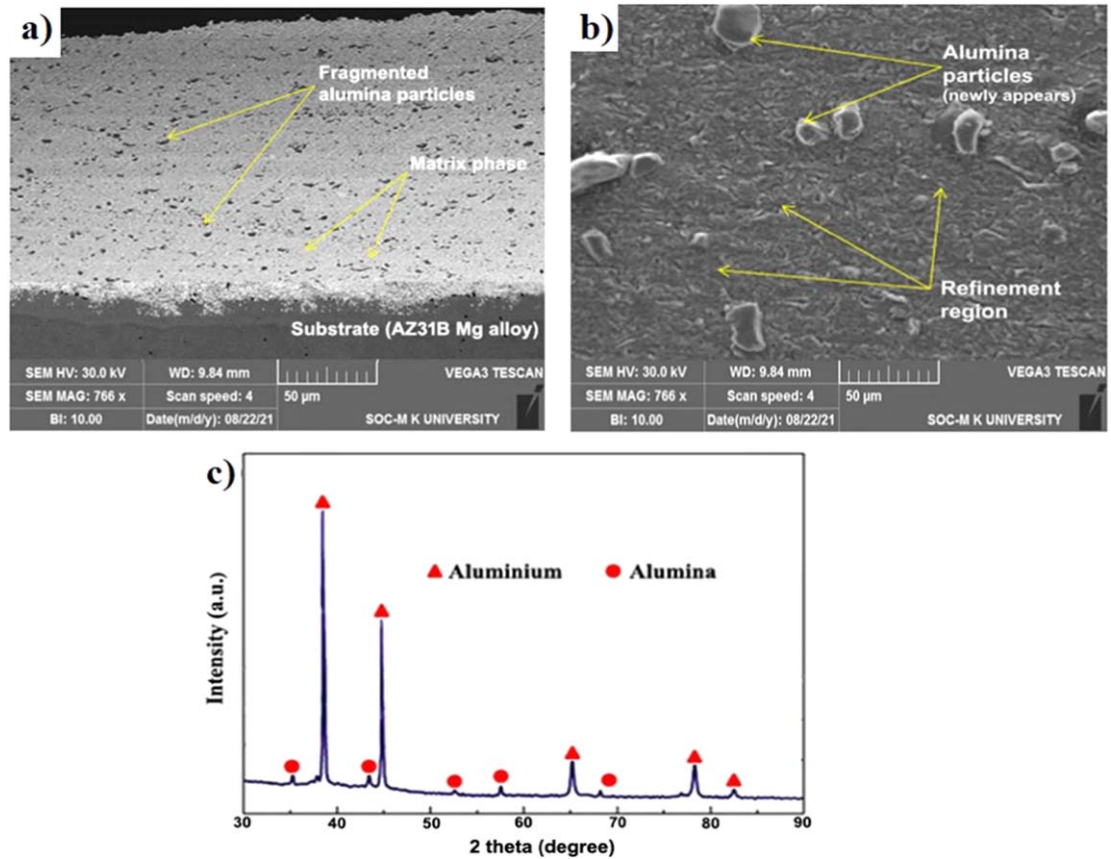
Figure 7. Scanning electron micrograph and XRD results of friction stir processed MMC coating: (a) Cross sectional view (b) Top surface view (c) XRD patten of friction stir processed MMC coatings (JCPDS card No. for aluminium: 85–1327 and for the alumina:10–0173).

aluminium oxide and metal elements [24, 25]. This behaviour leads to the negative corrosion properties of the cold sprayed coating. The FSP modifies the coating surface into a plastically deformed condition by distributing the aluminium oxide elements into the Al alloy phase, and the metal elements are diffused during the FSP by shear force [19–25]. It leads to a reduction of space in between the inner particles of the deposit. This reduced space in between the interior particles and the alumina particles that were refined and redistributed to enhance the corrosion resistance of the FSP treated cold sprayed MMC coatings.

3.2. Differential scanning calorimetry

The precipitate behaviour of the 2nd phase is identified through exothermal and endothermal heat flow. The region below the apex, or the amplitude apex, denotes the precipitation strength [23, 26]. Figure 8 illustrates the LPCS and FSPed MMC coatings of the DSC plot. For the matrix phase, there is the Guinier Preston Bagaryatskii region (GPB) and the S (S') phase. Then the GPB region was indicated by apex G and the S (S') phase by apex S.

The corrosion investigation on the matrix phase revealed the distributed S (S') phase had poor corrosion performance, particularly when the S (S') phase is

mainly located along the grain boundary [27]. Then it is considered the apex region A_1 as an LPCSed condition at a volume fraction of $fS_{(S')-A1}$. The relative fraction of S (S') precipitation in the FSPed condition is determined by the functional ratio between the S (S') precipitation apex zone A_2 of the FSPed and that of LPCSed [28]:

$$f_{S(S')-A1} = 1 - (A_2/A_1) + (A_2/A_1)f_{S(S')-A2} \quad (1)$$

At the friction stir technique, the volume fraction of the S (S') phase greatly decreased when compared to the LPCSed sample. At FSP, the dwell period at higher temperatures enhances, causing the development and coarsed S (S') phase to be low. As a result, the phase transition that occurs at the FSPed Al alloy matrix is advantageous for corrosion performance. So, it is a positive sign for the corrosion resistance of the MMC coatings.

3.3. Electrochemical corrosion behaviour
3.3.1. Potentio-dynamic polarization test
Figure 9 shows the OPC (open circuit potential) time response and cyclic polarisation plot for the AZ31B magnesium alloy, cold spayed MMC deposit, and friction stirred MMC deposit. The OCP value is used to determine the coatings corrosive behaviour in an
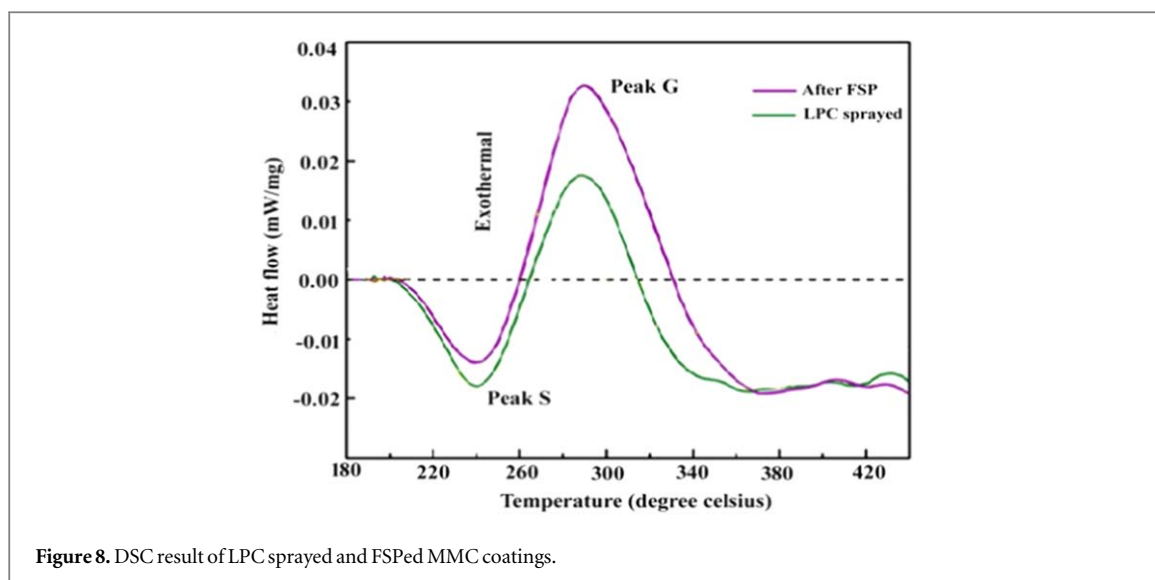
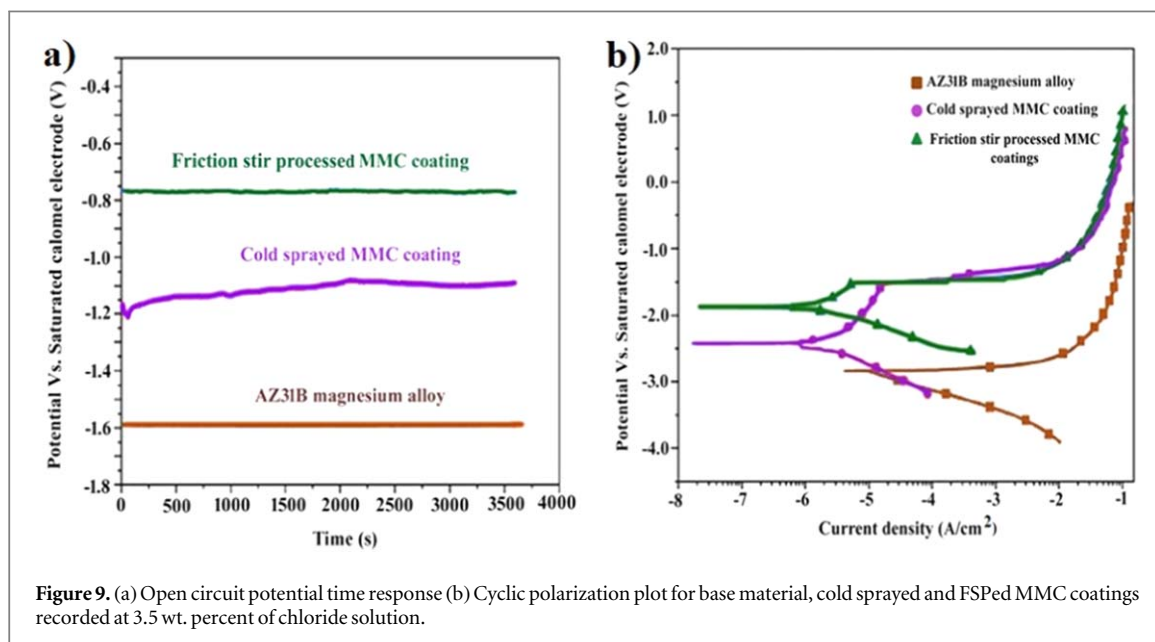**Figure 8.** DSC result of LPC sprayed and FSPed MMC coatings.

Figure 9. (a) Open circuit potential time response (b) Cyclic polarization plot for base material, cold sprayed and FSPed MMC coatings recorded at 3.5 wt. percent of chloride solution.

aqueous medium, with a greater OCP value indicating a lower corrosive behaviour as shown in figure 9(a), the OCP value of the AZ31B Mg alloy was lower throughout the entire corrosion process than that of the cold sprayed MMC and the friction stirred MMC coatings. This suggests that the corrosion resistance of AZ13B Mg alloy was considerably increased after cold sprayed MMC coatings. Furthermore, the OCP value of the friction stirred sample was greatly improved compared to the as sprayed coatings, indicating that after FSP, the degree of separation and dispersal of alumina in the Al alloy matrix was increased, the interface bonding between matrix and reinforcement phase was improved, and the corrosion resistance behaviour of FSP sample is seen in figure 10.

The corrosion potential (E_{corr}) and current density (I_{corr}) of specimens were computed and the results are reported in table 5. It discloses that the I_{corr} value of the cold sprayed and friction stir processed specimens was

substantially lower compared to the base material, implying that cold sprayed and FSP treated samples provide greater corrosion resistance. The value of E_{corr} for both cold sprayed and post treated specimens was greater compared to the uncoated substrate, indicating that the corrosion behaviour of the FSP and cold sprayed AZ31B Mg alloy in the NaCl solution can be reduced. When compared to the base material, the I_{corr} value of cold sprayed and FSP samples was reduced by 2 orders of magnitude. The OCP value and I_{corr} outcomes reveal that the cold sprayed and post sprayed samples can enhance the corrosion resistance of the AZ31B Mg alloy. Furthermore, the I_{corr} value of the friction stir processed sample (20.29×10^{-7} A cm^{-2}) was only half that of the cold sprayed MMC coating (46.59×10^{-7} A cm^{-2}), indicating that the friction stir processed sample has significantly superior corrosion resistance compared to the as sprayed coating. To validate the above statement, the
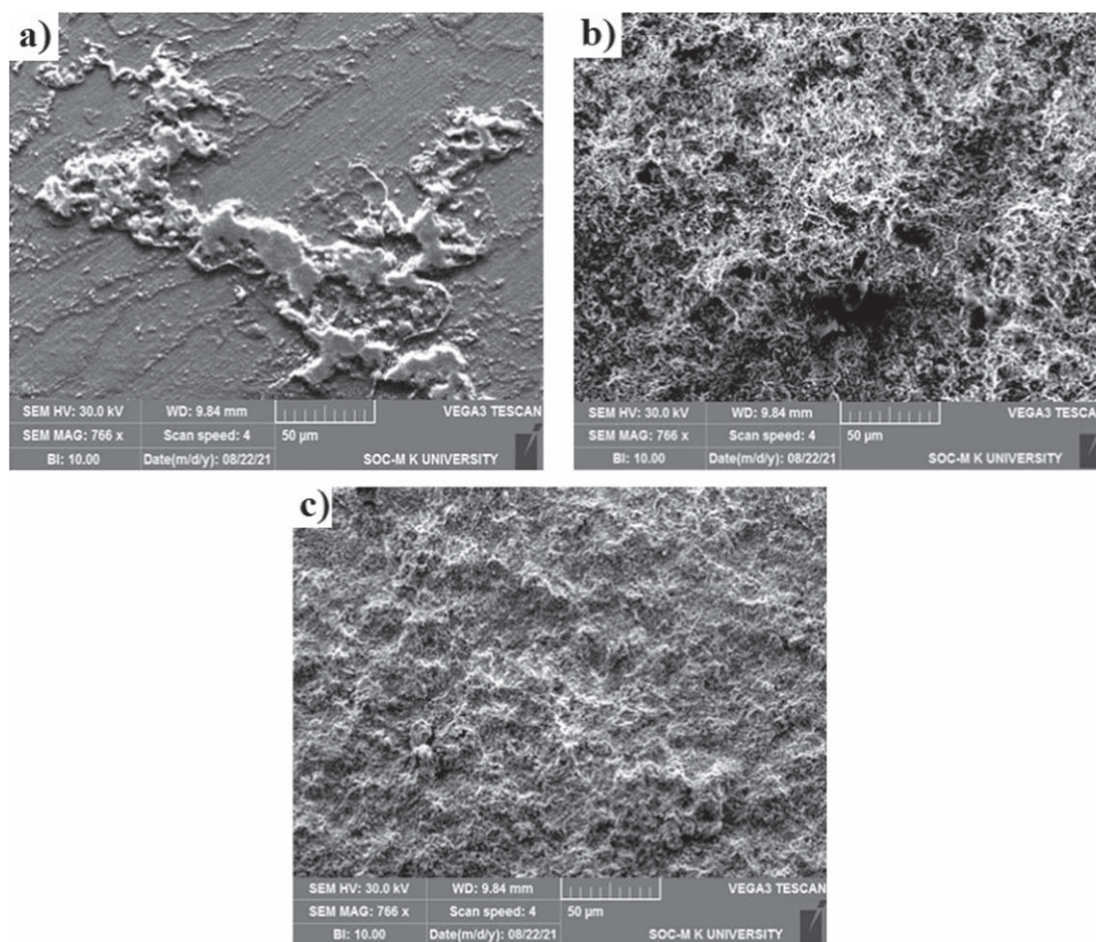
Figure 10. Corrosion morphology of the (a) substrate (b) cold sprayed and (c) FSPed MMC coatings after potentiodynamic polarization test.

Table 5. Results of Potentiodynamic polarization test.

Specimens	Corrosion potential, E_{corr} (Voltage)	Current density, I_{corr} (A cm^{-2})	Corrosion rate (mm year)$^{-1}$
AZ31B Mg alloy	$-.2.742$	11.24×10^{-5}	2.52
Cold sprayed	-2.224	46.59×10^{-7}	1.66
FSP	-1.939	20.29×10^{-7}	0.82

corrosion morphology of the cold sprayed and post treated specimens was shown in figure 10.

3.3.2. Electrochemical impedance spectroscopy (EIS)

An EIS was utilised to evaluate the corrosion behaviour and electrochemical mechanism of the Al alloy/alumina MMC coatings. Figure 11 illustrates the CSed and FSPed MMC deposits experimentally obtained by Nyquist and Bode plot. The Nyquist plot reveals that for all the two specimens having two different semicircles, it detonates the pair of capacitive curves and two times constant. Although the two capacitive curves overlapped, the two-time constants are indistinguishable from the CS sample. Figure 11(a) demonstrates the semicircle amplitudes in the following sequence: CS > FSP. From this, the FSP run attained the maximum impedance modulus, which provided excellent corrosion performance as shown in figure 12(b). This is due to the plastically deformed state of the coatings by the thermo mechanical process of the FSP and the interface voids between the matrix (Al alloy) and secondary (alumina) phase being greatly reduced. The generation of the EIS result for the CSed and FSPed specimens, the electrical equivalent circuit (EEC) at two-time constants is shown in figure 13. R_S is the solution resistance, R_t is charge transformation resistance at the deposit-electrolyte interfacial, with the constant phase element CPE$_d$ at normal frequencies. Rf is the interior MMC coating resistance. R_f is a lower frequency parallel to CPE$_f$ [23, 26].

Table 6 reveals that the R_t of the CSed sample is smaller. At the completion of the FSP run, the result of
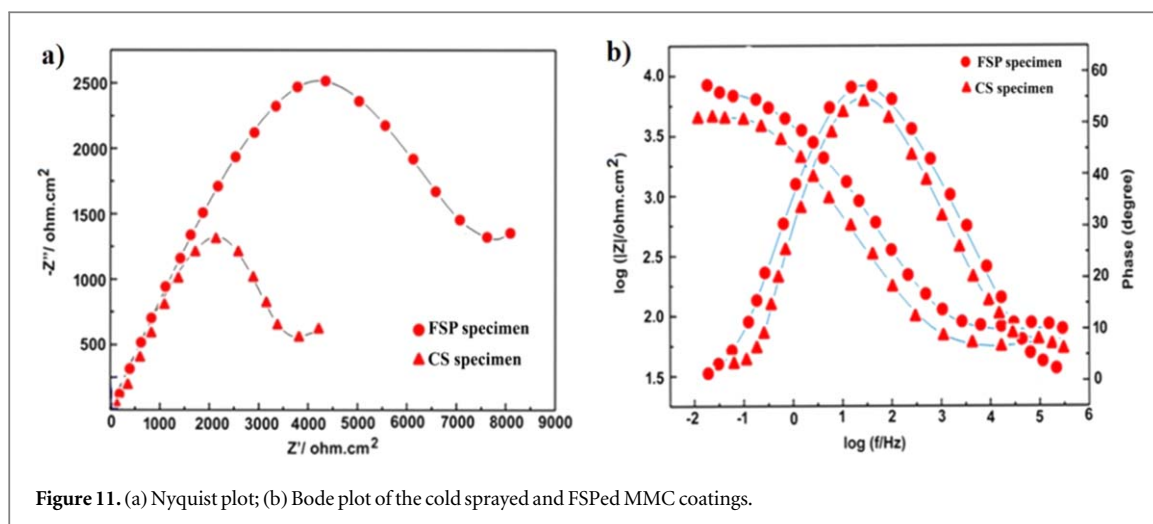
Figure 11. (a) Nyquist plot; (b) Bode plot of the cold sprayed and FSPed MMC coatings.
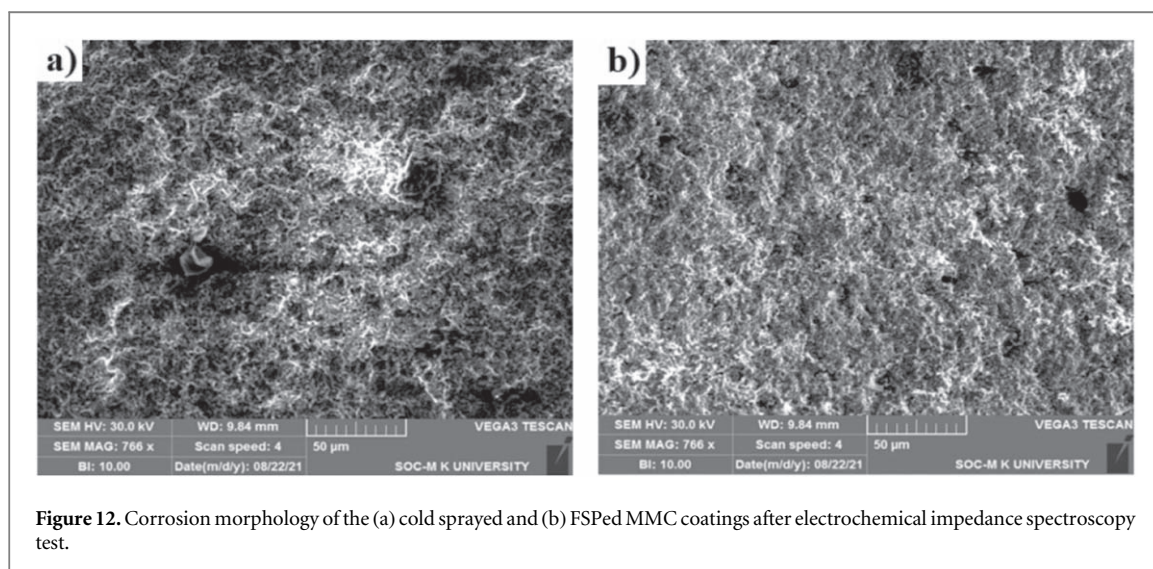

Figure 12. Corrosion morphology of the (a) cold sprayed and (b) FSPed MMC coatings after electrochemical impedance spectroscopy test.
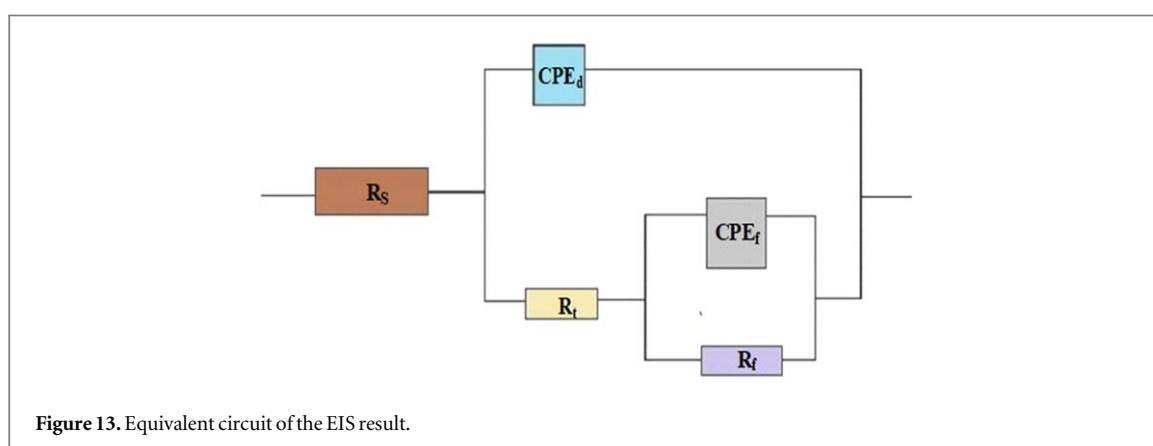

Figure 13. Equivalent circuit of the EIS result.

R_t increased hugely. In contrast, the Rf reveals a decreasing tendency in the FSP runs. Based on the previous studies [23, 26], summing the R_t and R_f assists in understanding the properties of corrosion behaviour. The FSP run greatly improves the corrosion performance of the CSed Al alloy/alumina deposit, as illustrated in figure 12(b). This enhancement is due to

reduced space in between the interior particles and the alumina particles that were refined and redistributed around the coating surface.

Prior studies [23–34] have shown that the level of R_t is determined by the coating properties. The R_t value increases due to the massive enhancement in the coated region after FSP. According to the surface

Table 6. Results of electrochemical impedance spectroscopy (EIS) test.

Samples	Rs (ohm.cm^2)	CPE$_d$ (F cm^{-2})	n$_d$	R$_t$ (kohm.cm^2)	CPE$_f$ (F.cm^{-2})	n$_f$	R$_f$ (kohm.cm^2)	R$_t$ + R$_f$ (kohm.cm^2)
CSP	44.11	0.37×10^{-4}	0.78	3.75	55.30×10^{-4}	0.91	1.83	5.58
FSP	42.16	0.37×10^{-4}	0.73	7.86	49.86×10^{-4}	1.01	1.69	9.55

morphology analysis (figures 7(a) and (b)), the excellent surface structure of the friction stir MMC deposit can be attributed to the aluminium oxide elements being refined and redistributed excellently in the coated surface, and the spaces between the inner splat boundaries and the S(S') phase volume fraction were also reduced. In the cold sprayed Rt was reduced due to the higher angle grain boundary on the surface of the Al alloy/alumina composite deposit [23], and the presence of aluminium oxide in cold sprayed MMC coatings was expected to lower the area that can be assaulted by an electrolyte. However, the assault on the aluminium oxide elements was stronger due to the weak interface bond between aluminium oxide and metal elements, resulting in poor corrosion performance in the cold sprayed state [21] as shown in the figure 12(a).

After FSP, the R_f value decreases predominantly owing to the breaking of oxide films in the inner region of the MMC deposit, caused by the weak interfacial contact between the elements of the interior deposit. [23, 31]. It is summed up that the foremost development mechanism of corrosion protection after FSP is the enhancement of the coating surface properties. It is based on the increase in R_t value. EIS data reveals that R_t was high for post treated samples. Therefore, friction stirred Al/alumina metal matrix composite coatings show excellent corrosion resistance compared to as sprayed conditions as shown in figure 12.

4. Conclusions

1. The FSP was successfully performed on LPCSPed Al-Al$_2$O$_3$ MMC coating deposited on AZ31B magnesium alloy without any defects.

2. The porosity of MMC coating is reduced to 0.5% with a significant increase in microhardness up to 155 HV by FSP compared to as-sprayed coated samples. It is correlated to the refining of alumina oxide elements on the coating surface.

3. The volume fraction of S' phase is dramatically reduced after FSP on the coated surface resulting in a significant improvement in the corrosion resistance of the FSP sample as compared to the coated sample.

4. The FSP samples exhibited superior corrosion resistance compared to the cold sprayed sample. It is attributed to the enhanced interfacial bonding between the matrix and reinforcement phase.

5. The degree of separation and dispersion of alumina in the Al alloy matrix is increased by the shear force generated through the FSP tool on the coating surface.

6. The superior corrosion resistance and hardness of Al-Al$_2$O$_3$ MMC coated on AZ31B Mg alloy achieved using FSP proves its viability in aerospace and automotive applications for helicopter rotor fittings and aircraft engine mounts, automobiles engine blocks and housing for transmissions.

Data availability statement

All data that support the findings of this study are included within the article (and any supplementary files).

ORCID iDs

Ashokkumar Mohankumar ⬤ https://orcid.org/0000-0002-8926-4103
Deepak Sampathkumar ⬤ https://orcid.org/0000-0002-4704-5367

References

[1] Thirumalaikumarasamy D, Shanmugam K and Balasubramanian V 2014 Comparison of the corrosion behaviour of AZ31B magnesium alloy under immersion test and potentiodynamic polarization test in NaCl solution *Journal of Magnesium and Alloys* **2** 36–49

[2] Tan J and Ramakrishna S 2021 Applications of magnesium and its alloys: a review *Applied Sciences* **11** 6861

[3] Maev R G and Leshchynsky V 2018 Cold-spray coatings: recent trends and future perspectives *Low-Pressure Cold Spray* 95–142

[4] Mohankumar A, Duraisamy T, Sampathkumar D, Ranganathan S, Balachandran G, Kaliyamoorthy M and Mulugeta L 2022 Optimization of cold spray process inputs to minimize porosity and maximize hardness of metal matrix composite coatings on AZ31B magnesium alloy *J. Nanomater.* 2022

[5] Yang G J, Li C J, Han F, Li W Y and Ohmori Low A 2008 temperature deposition and characterization of TiO$_2$ photocatalytic film through cold spray *Appl. Surf. Sci.* **254** 3979–82

[6] Ashokkumar M, Thirumalaikumarasamy D, Thirumal P and Barathiraja R 2021 Influences of mechanical, corrosion, erosion and tribological performance of cold sprayed coatings a review *Mater. Today Proc.* **46** 7581–7

[7] Kaczmarek L, Kyzioł K, Sawicki J, Stegliński M, Radziszewska H, Szymański W and Zawadzki P 2013 The influence of chemical groups on the mechanical properties of SiCNH coatings deposited on 7075 aluminum alloy *Thin Solid Films* **534** 15–21

[8] Mathanbabu M, Thirumalaikumarasamy D, Thirumal P and Ashokkumar M 2021 Study on thermal, mechanical, microstructural properties and failure analyses of lanthanum

zirconate based thermal barrier coatings: a review *Mater. Today Proc.* **46** 7948–54

[9] Mathivanan K, Thirumalaikumarasamy D, Thirumal P and Ashokkumar Investigate M 2022 the corrosion properties of stellite coated on AZ91D alloy by plasma spray technique *Thermal Science* **26** 911–20

[10] Mathivanan K, Thirumalaikumarasamy D, Ashokkumar M, Deepak S and Mathanbabu M 2021 Optimization and prediction of AZ91D stellite-6 coated magnesium alloy using Box Behnken design and hybrid deep belief network *Journal of Materials Research and Technology* **15** 2953–69

[11] Yu M, Suo X, Li W, Wang Y and Liao H 2014 Microstructure, mechanical property and wear performance of cold sprayed Al5056/SiCp composite coatings: effect of reinforcement content *Appl. Surf. Sci.* **289** 188–96

[12] Spencer K, Fabijanic D M and Zhang M X 2009 The use of Al–Al₂O₃ cold spray coatings to improve the surface properties of magnesium alloys *Surf. Coat. Technol.* **204** 336–44

[13] Pialago E, Kwon O and Park C W 2015 Cold spray deposition of mechanically alloyed ternary Cu-CNT-SiC composite powders *Ceram. Int.* **41** 6764–75

[14] Huang C J, Li W Y, Feng Y, Xie Y C, Planche M P, Liao H L and Montavon G 2017 Microstructure evolution and mechanical properties enhancement of a cold-sprayed Cu-Zn alloy coating with friction stir processing *Mater. Charact.* **125** 76–82

[15] Qiu X, Wang J Q, Tang J R, Gyansah L, Zhao Z P and Xiong T Y 2018 Microstructure, microhardness and tribological behavior of Al₂O₃ reinforced A380 aluminum alloy composite coatings prepared by cold spray technique *Surf. Coat. Technol.* **350** 391–400

[16] Xie C, Li H, Zhou X and Sun C 2019 Corrosion behavior of cold sprayed pure zinc coating on magnesium *Surf. Coat. Technol.* **374** 797–806

[17] Gawel R, Kyzioł K, Jurasz Z and Grzesik Z 2018 Oxidation resistance of valve steels covered with thin SiC coatings, obtained by RF CVD *Corros. Sci.* **145** 16–25

[18] Huang R, Sone M, Ma W and Fukanuma H 2015 The effects of heat treatment on the mechanical properties of cold-sprayed coatings *Surface and Coatings Technology* **261** 278–88

[19] Ma Z Y 2008 Friction stir processing technology: a review *Metallurgical and Materials Transactions* A **39** 642–58

[20] Khodabakhshi F, Marzbanrad B, Shah L H, Jahed H and Gerlich A P 2017 Friction-stir processing of a cold sprayed AA7075 coating layer on the AZ31B substrate: structural homogeneity, microstructures and hardness *Surf. Coat. Technol.* **331** 116–28

[21] Hodder K J, Izadi H, McDonald A G and Gerlich A P 2012 Fabrication of aluminum-alumina metal matrix composites via cold gas dynamic spraying at low pressure followed by friction stir processing *Materials Science and Engineering* **556** 114–21

[22] Huang C J, Li W Y, Yu M, Planche M, Liao H and Montavon G 2016 Modification of a cold sprayed SiCp/Al5056 composite coating by friction stir processing *Surf. Coat. Technol.* **296** 69–75

[23] Yang K, Li W, Xu Y and Yang X 2019 Using friction stir processing to augment corrosion resistance of cold sprayed AA2024/Al₂O₃ composite coatings *J. Alloys Compd.* **774** 1223–32

[24] Peat T, Galloway A, Toumpis A, McNutt P and Iqbal N 2017 The erosion performance of cold spray deposited metal matrix composite coatings with subsequent friction stir processing *Appl. Surf. Sci.* **396** 1635–48

[25] Silva F S, Bedoya J, Dosta S, Cinca N, Cano I G, Guilemany J M and Benedetti A V 2017 Corrosion characteristics of cold gas spray coatings of reinforced aluminum deposited onto carbon steel *Corros. Sci.* **114** 57–71

[26] Bai Y, Wang Z H, Li X B, Huang G S, Li C X and Li Y 2017 Corrosion behaviour of low pressure cold sprayed Zn-Ni composite coatings *J. Alloys Compd.* **719** 194–202

[27] Pang J J, Liu F C, Liu J, Tan M J and Blackwood D J 2016 Friction stir processing of aluminium alloy AA7075: microstructure, surface chemistry and corrosion resistance *Corros. Sci.* **106** 217–28

[28] Tao Y S, Xiong T Y, Sun C, Kong L Y, Cui X Y, Li T F and Song G L 2010 Microstructure and corrosion performance of a cold sprayed aluminium coating on AZ91D magnesium alloy *Corros. Sci.* **52** 3191–7

[29] Sidhar H and Mishra R S 2016 Aging kinetics of friction stir welded Al-Cu-Li-Mg-Ag and Al-Cu-Li-Mg alloys *Mater. Des.* **110** 60–71

[30] Alexopoulos N D, Velonaki Z, Stergiou C I and Kourkoulis S K 2016 The effect of artificial ageing heat treatments on the corrosion-induced hydrogen embrittlement of 2024 (Al-Cu) aluminium alloy *Corros. Sci.* **102** 413–24

[31] Hassani-Gangaraj S M, Moridi A and Guaglinao M 2015 Critical review of corrosion protection by cold spray coatings *Surf. Eng.* **31** 803–15

[32] Rao Y, Wang Q, Oka D and Ramachandran C S 2020 On the PEO treatment of cold sprayed 7075 aluminum alloy and its effects on mechanical, corrosion and dry sliding wear performances thereof *Surface and Coatings Technology* **383** 125271

[33] Rao Y, Wang Q, Chen J and Ramachandran C S 2021 Abrasion, sliding wear, corrosion, and cavitation erosion characteristics of a duplex coating formed on AZ31 Mg alloy by sequential application of cold spray and plasma electrolytic oxidation techniques *Materials Today Communications* **26** 101978

[34] Tan K, Markovych S, Hu W, Wang Y, Shorinov O and Wang Y 2021 On the characteristics of cold spray technology and its application in aerospace industries *In IOP Conference Series: Earth and Environmental Science* **719** 032023